CH-π Interactions Promote the Conversion of Hydroxypyruvate in a Class II Pyruvate Aldolase

Marsden, Stefan R.; Mestrom, Luuk; Bento, Isabel; Hagedoorn, Peter Leon; McMillan, Duncan G.G.; Hanefeld, Ulf

DOI
10.1002/adsc.201900205

Publication date
2019

Document Version
Final published version

Published in
Advanced Synthesis and Catalysis

FULL PAPER DOI: 10.1002/adsc.201900205 Advanced Synthesis & Catalysis

CH-π Interactions Promote the Conversion of Hydroxypyruvate in a Class II Pyruvate Aldolase

Stefan R. Marsden,[a, b] Luuk Mestrom,[a] Isabel Bento,[b,*] Peter-Leon Hagedoorn,[a] Duncan G. G. McMillan,[a] and Ulf Hanefeld[a,*]

[a] Biokatalyse, Afdeling Biotechnologie, Technische Universiteit Delft, van der Maasweg 9, 2629HZ Delft, The Netherlands
+31 15 278 9304
E-mail: U.hanefeld@tudelft.nl
[b] EMBL Hamburg, Notkestrasse 85, 22607 Hamburg, Germany
E-mail: ibento@embl-hamburg.de

Manuscript received: February 12, 2019; Revised manuscript received: April 1, 2019;
Version of record online: May 14, 2019

Supporting information for this article is available on the WWW under https://doi.org/10.1002/adsc.201900205

Abstract: The class II hydroxy ketoacid aldolase A5VH82 from *Sphingomonas wittichii* RW1 (*Sw*HKA) accepts hydroxypyruvate as nucleophilic donor substrate, giving access to synthetically challenging 3,4-dihydroxy-α-ketoacids. The crystal structure of holo-*Sw*HKA in complex with hydroxypyruvate revealed CH-π interactions between the C–H bonds at C3 of hydroxypyruvate and a phenylalanine residue at position 210, which in this case occupies the position of a conserved leucine residue. Mutagenesis to tyrosine further increased the electron density of the interacting aromatic system and effected a rate enhancement by twofold. While the leucine variant efficiently catalyses the enolisation of hydroxypyruvate as the first step in the aldol reaction, the enol intermediate then becomes trapped in a disfavoured configuration that considerably hinders subsequent C–C bond formation. In *Sw*HKA, micromolar concentrations of inorganic phosphate increase the catalytic rate constant of enolisation by two orders of magnitude. This rate enhancement was now shown to be functionally conserved across the structurally distinct $(\alpha/\beta)_8$ barrel and αββα sandwich folds of two pyruvate aldolases. Characterisation of the manganese (II) cofactor by electron paramagnetic resonance excluded ionic interactions between the metal centre and phosphate. Instead, histidine 44 was shown to be primarily responsible for the binding of phosphate in the micromolar range and the observed rate enhancement in *Sw*HKA.

Keywords: pyruvate; hydroxypyruvate; aldolase; CH-π interactions; phosphate activation

Introduction

Aldolase catalysed asymmetric C–C bond formation plays a pivotal role in the synthesis of many chiral building blocks,[1] natural compounds,[2] pharmaceuticals[3] and has been industrially applied on a multi ton scale.[4] Due to this wide-ranging utility, its relevance for synthetic chemistry is well recognized.[5] There are two distinct types of aldolases that are classed by their respective mode of action. Class I aldolases function *via* a Schiff base mechanism involving a lysine residue,[6] while class II aldolases require a divalent metal cation as cofactor for substrate binding and activation.[7] In general, aldol reactions are fully reversible *via* the same reaction pathway. In nature, such retro-aldol reactions are found in biodegradation pathways of aromatic compounds such as phenols, biphenyls and lignin derived metabolites, which then can be metabolised.[8] For synthetic purposes, aldolase catalysed reactions with pyruvate are well established and give straightforward access to 4-hydroxy-α-ketoacids.[1a,9] Unfortunately, wild type pyruvate aldolases typically show a strict requirement for a single donor substrate, which considerably limits their product scope. To address this issue, de Berardinis et al. conducted an extensive screening of 571

aldolases, of which only 19 enzymes showed an observable promiscuity towards hydroxypyruvate (HPA) as nucleophilic donor substrate.[10] In particular, aldolase A5VH82 from *Sphingomonas wittichii* RW1 showed good conversions, giving new access to several 3,4-dihydroxy-α-ketoacids by variation of the acceptor aldehyde. Intrigued by its unusual activity, we set out to elucidate the molecular basis behind the enzyme's widened donor substrate scope and to conduct an extensive biochemical and structural characterisation. Our findings motivated us to denote this enzyme as a hydroxy ketoacid aldolase (*Sw*HKA, Scheme 1).

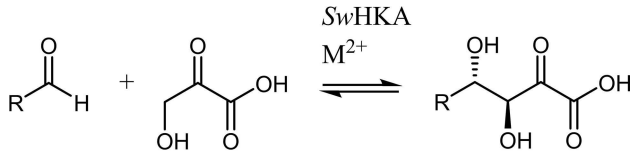

Scheme 1. *Sw*HKA catalysed aldol coupling of hydroxypyruvate with an acceptor aldehyde to afford a 3*(S)*,4*(S)*-dihydroxy-α-ketoacid.[10]

A first indication of phosphate being involved in the catalytic mechanism of class II pyruvate aldolases was given by the crystal structure of the 2-dehydro-3-deoxy-galactarate aldolase from *Escherichia coli* (DDG, 1dxf.pdb). Based on the apparent absence of catalytically active amino acid residues and an increased activity in phosphate buffer, the authors proposed a reaction mechanism which involved inorganic phosphate as the catalytic base.[11] This hypothesis has since been challenged by observations for the homologous enzyme HpaI (44% sequence identity with DDG) where lower activities were found in the presence of phosphate.[12] While a recent study on the class II HMG/CHA pyruvate aldolase described a 10-fold rate enhancement by inorganic phosphate, these findings were attributed to the enzyme's distinct structure (αββα sandwich fold in the HMG/CHA aldolase[13] *vs.* an $(\alpha/\beta)_8$ barrel fold in the DDG aldolase;[11] 16.8% shared sequence identity).[14] Here we present new insights into the mode of phosphate activation by identifying the key residues that are involved in the binding of phosphate and the concomitant rate enhancement. Our results show that phosphate activation is functionally conserved within the same order of magnitude in the $(\alpha/\beta)_8$ barrel fold of *Sw*HKA and thereby not a unique property of the αββα sandwich fold. Furthermore, using the crystal structure of holo-*Sw*HKA in complex with hydroxypyruvate, we were able to demonstrate CH-π interactions between residue F210 and HPA to be responsible for its conversion. Based on this, we could then rationally devise a variant of two-fold improved turnover rate.

Results and Discussion

Biocatalyst Production

The *Sw*HKA gene was codon optimised for recombinant expression in *E. coli* BL21(DE3) and a purified protein yield of up to 75 mg/L medium was obtained upon single-step metal affinity purification *via* its N-terminal His_6-tag. Notably, gene expression in *E. coli* BL21Star(DE3) yielded approximately 2.5 g/L of insoluble inclusion bodies with *Sw*HKA as its main constituent, while only 10–20 mg/L was present in its soluble form. The inclusion bodies were purified with sodium deoxycholate and subsequently re-dissolved in urea, but no functional enzyme could be recovered. Cheap and high yielding biocatalyst production from purified inclusion bodies was therefore not possible. Overall, gene expression in *E. coli* BL21(DE3) gave higher yields of soluble protein. For crystallisation studies, the soluble enzyme was further purified by size exclusion chromatography resulting in a single peak corresponding to a hexameric homo-oligomer (27.4 kDa × 6 = 164.4 kDa), a commonly found structural state of other class II pyruvate aldolases.[11,15]

Crystal Structure of Mg^{2+}-*Sw*HKA (6r62.pdb)

The crystal structure of holo-*Sw*HKA in complex with hydroxypyruvate was determined at 1.55 Å resolution. The final structural model corresponds to a monomeric subunit (Figure S1) and includes all 251 amino acid residues plus one histidine residue from the His_6-tag. Additionally, one Mg^{2+} ion and one hydroxypyruvate moiety were found fully occupied in the electron-density maps, together with 352 solvent molecules. The monomeric subunit shows an $(\alpha/\beta)_8$ triosephosphate isomerase (TIM) fold, similar to the structures of the homologues 4-hydroxy-2-oxo-heptane-1,7-dioate aldolase (HpaI)[15] and 2-dehydro-3-deoxygalactarate aldolase (DDG).[11] The 8th α-helix extends out of the β-barrel and packs onto a β-sheet of a neighbouring two-fold related subunit to form a domain-swapped dimer (Figure S2). In agreement with previous results from size exclusion chromatography, a final hexameric assembly was obtained by application of the 3-fold crystallographic symmetry to this domain swapped dimer. (Figure S3, S4). Comparison with the homologous enzymes HpaI (rmsd 1.54 Å for 243/251 aligned residues) and DDG (rmsd 1.61 Å for 243/251 aligned residues) indicated, that the overall fold is conserved in *Sw*HKA. The active site is located inside a cavity close to the *C*-terminus, and comprises of residues from two different monomeric subunits and a metal cluster (Figure 1). The Mg^{2+} ion is coordinated by two carboxylate groups from residues E145 and D171 in a monodentate fashion, two water molecules (W1, W2) and the bidentate binding of hydroxypyruvate *via* its

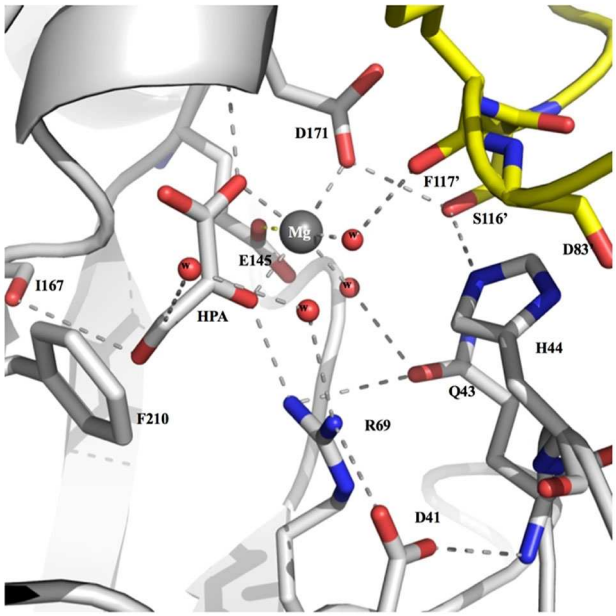

Figure 1. Representation of the relevant active site residues in Mg^{2+}-*Sw*HKA (6r62.pdb). The backbones of the two monomeric subunits that form the active site are coloured in grey and yellow. Figures were created with PyMOL.[16]

carbonyl and the carboxylate group completes the octahedral geometry.

HPA therefore coordinates the metal cofactor in a similar way as pyruvate in homologous structures.[11,15] The carboxylate group in HPA is located within hydrogen bond distance to the backbone NH and side chain hydroxyl of T170. The carbonyl group in HPA forms a hydrogen bond with R69 and its C3 hydroxyl group is within hydrogen bond distance of the carbonyl backbone of I167. Furthermore, a well-ordered water molecule is observed at 3 Å distance from C3 in HPA. This water molecule constitutes a good candidate for the catalytic deprotonation at C3, similar to the proposed role of water in the structure of pyruvate bound HpaI (4b5u.pdb).[15] This bridging interaction is necessary due to the absence of proximal amino acid residues for a direct deprotonation. Notably, F210 replaces a conserved leucine residue (L212 and L216 for HpaI and DDG, respectively) as the most apparent difference in active site geometries. The C3 C–H bonds in HPA are oriented towards the aromatic system of F210 and establish CH-π interactions.[17] This hydrophobic region was previously proposed to flank the aldehyde binding locus.[15] Another important and conserved residue in the active site is H44 (H45 and H50 in HpaI and DDG, respectively). H44 is located within hydrogen bond distance of D83' in the symmetry related subunit and of a water molecule that coordinates the Mg^{2+} ion. Together with the loop region that comprises of residues 115′ to 120′ in the symmetry related molecule, D83′ is involved in a hydrogen bond network that contributes to the integrity of the active site. H44 forms hydrogen bonds with R120′ and D171. Furthermore, D171 forms hydrogen bonds with F117′, S116′ and one of the water molecules from the Mg^{2+} coordination sphere. Although this loop shows low sequence conservation among the homologous enzymes, it maintains the active site configuration *via* the hydrogen bond network.

Biochemical Characterisation

In class II aldolases, divalent metal ions play a central role in catalysis.[7] For *Sw*HKA, a slight preference for Mn^{2+} over Mg^{2+} and Co^{2+} was previously reported, but no dissociation constants or kinetic parameters were measured.[10] Therefore, the metal dependent activity of the enzyme was screened, including Ni^{2+}, Ca^{2+} and Zn^{2+}, with the latter being commonly found in the dihydroxyacetonephosphate specific subgroup of class II aldolases.[18] The highest activity was observed with Mn^{2+} as cofactor, followed by Mg^{2+} with 83% of the activity of Mn^{2+} (Figure 2). While rather similar in rate, a strong preference for Mn^{2+} over Mg^{2+} was observed with respect to their apparent binding constants, with a K_d of 3.3 ± 0.6 μM for Mn^{2+} in contrast to 58.4 ± 4.1 μM for Mg^{2+}. These results are of particular interest, since solvated Mg^{2+} and Mn^{2+} ions are known to be poor Lewis acid catalysts in aqueous media.[19] A previous study on the Mn^{2+} containing enzyme *Gt*HNL suggested a distorted octahedral coordination geometry to be responsible for

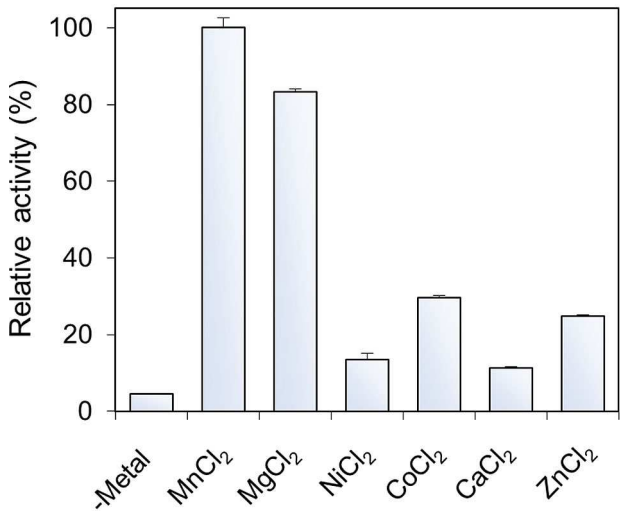

Figure 2. Metal dependent relative activities of *Sw*HKA under metal saturated conditions (10 mM M^{2+}, 20 mM TEOA, pH 8.0). Activities were determined for the retro-aldol type decarboxylation of oxaloacetate by a NADH/LDH coupled enzyme assay and the results were normalized for Mn^{2+}.

Table 1. Overview of apparent metal/phosphate dissociation constants and the corresponding saturation kinetics v_{sat} under standard assay conditions (0.5 mM oxaloacetate).

Enzyme	M^{2+}	Pi	v_{sat} (U/mg)	$K_{d,M2+}$ (μM)	$K_{d,Pi}$ (mM)
WT	Mn^{2+}	–	2.15 ± 0.09	3.3 ± 0.6	–
WT	Mg^{2+}	–	1.65 ± 0.03	58.4 ± 4.1	–
WT	Mn^{2+}	+	27.0 ± 0.67	6.5 ± 0.7	0.18 ± 0.04
WT	Mg^{2+}	+	17.21 ± 0.29	158 ± 12	0.13 ± 0.02
H44A	Mn^{2+}	–	0.78 ± 0.01	n.d.[a]	–
H44A	Mn^{2+}	+	2.23 ± 0.08	n.d.[a]	6.22 ± 0.53

[a] n.d. = not determined

the increased Lewis acidity, where the connecting line between the two tops of the square-based pyramid deviates from the expected angle of 180°.[20] A similar deviation was also observed in the crystal structure of holo-*Sw*HKA for the Mg^{2+} cluster (6r62.pdb).

To determine the pH optimum, the enzyme activity was measured in several buffer systems over a range from 5.5 to 8.25 and the optimum was found at pH 6.75. Notably, long-term storage of the enzyme at −20 °C required alkaline conditions (pH ≥ 7.5), under which the enzyme retained full activity for more than one month (data not shown). Incubation in potassium phosphate buffer substantially increased the reaction rate in comparison with other buffer salts. Analysis over a broad range of concentrations revealed a considerable affinity towards phosphate, with an apparent dissociation constant of $K_{d,Pi}$ = 175 ± 36 μM. This observation was of particular interest, since phosphate buffers were reported to exhibit an adverse effect on the activity of class II aldolases in several other cases,[12,21] with only one exception.[14] Strikingly,

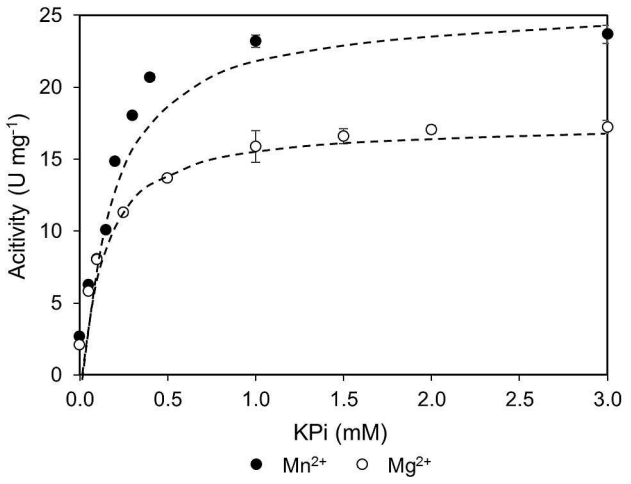

Figure 3. Catalytic rate enhancement in *Sw*HKA by the presence inorganic phosphate under metal saturated conditions (0.1 mM Mn^{2+}, 1 mM Mg^{2+}, 5 mM TEOA, pH 7.5). Rates were determined by the coupled enzyme assay.

even minor concentrations of phosphate significantly increased the reaction rate up to 13-fold under standard assay conditions, from 2.1 U/mg to v_{sat} = 27.1 U/mg following saturation kinetics with respect to phosphate (Figure 3). The metal dissociation constants for Mn^{2+} and Mg^{2+} were unaffected by the presence/absence of phosphate, rendering a direct ionic interaction unlikely (Table 1). Henceforth, we directed our attention towards the two positively charged active site residues R69 and H44, which appeared to be likely candidates involved in phosphate binding. While H44 also plays a structural role by interacting with D83 from another dimer, mutant H44A still displayed 40% (0.78 ± 0.01 U/mg) residual activity in the absence of phosphate.

However, the mutant's affinity towards phosphate was reduced 36-fold with $K_{d,Pi}$ = 6.22 ± 0.53 mM and the related rate enhancement was only 3-fold (2.23 ± 0.08 U/mg, Figure S22). Since both phosphate binding and activation are not completely lost by a replacement with alanine, H44 seems to be primarily, but not solely responsible for the observed activation of *Sw*HKA by inorganic phosphate. In agreement with previous studies, a complete loss of activity was observed for the R69A mutant both in the absence and presence of saturating concentrations of phosphate. These findings demonstrate, that neither H44 in combination with P_i, nor phosphate alone can act as the catalytic base and that R69 is required.

Despite a low dissociation constant, measurements of inorganic phosphate after metal affinity chromatography did not support its enzyme bound co-purification, indicating that while beneficial, phosphate is not essential for catalysis. These results are consistent with previous studies, where a structural molecule of water was identified as the catalytic base, due to the lack of proximal amino acid residues for a direct deprotonation at C3 in the substrate.[9a,12,15,22] Ultimately, elevated concentrations of phosphate (> 10 mM KPi) were found to have a negative impact on the reaction rate (Figure S23). We propose this to be due to the typically low solubility of divalent metal phosphates, which deprives the active site from its metal cofactor.[23] Notably, a higher rate of reaction can still be observed for states where the apoenzyme predominates, due to the rate enhancing effect of phosphate. This issue was addressed experimentally by using the minimal concentrations of metal and phosphate that are required for establishing saturating conditions. These findings plausibly clarify the previous misconception of the effect of phosphate in literature, where it typically was added in a large excess of 50–1000 molar equivalents with respect to the metal.[12,21,22d] Finally, we would like to mention that amine buffers are known organocatalysts for the transketolase-like conversion of hydroxypyruvate.[24] Using decarboxylation as driving force, this reaction then affords a racemic dihydrox-

yketone in place of the desired aldol product.[25] This considerably limits the range of buffer systems which would allow for selective aldol reactions with hydroxypyruvate at neutral pH. In theory, structural analogues of phosphate with matching pKa values should also be able to act as the catalytic base. Indeed, AsO_4^{3-} and VO_4^{3-} were previously shown to similarly activate the HMG/CHA aldolase, while SO_4^{2-} and MoO_4^{2-} did not.[14] A brief overview of phosphate analogues and their corresponding pKa values is given in Table S3.

EPR Characterisation of the Metal Centre

To further elucidate the interplay between the metal cofactor, inorganic phosphate and the substrates, the metal centre was analysed by EPR (Figure 4). Mn^{2+} is paramagnetic, characterised by a high spin $S=5/2$ and the hyperfine coupling of the nuclear spin $I=5/2$ of ^{55}Mn (100% natural abundance) and was therefore chosen as the metal cofactor for EPR experiments. The Mn^{2+} EPR is characteristic, as it is a unique case where the zero-field splitting (which is independent of the magnetic field) is smaller or equal to the Zeeman interaction (dependent on the magnetic field). This is contrary to most other paramagnetic metal ions, for which the zero field splitting is much larger, e.g. high spin Fe^{3+} ($S=5/2$). The spectrum is very broad because of five allowed transitions with each $\Delta m_s=1$, and each of these transitions is split into six lines due to the ^{55}Mn hyperfine coupling. Normally, Mn^{2+} is dominated by the $m_s=-1/2$ to $m_s=+1/2$ transition, which results in a broad signal around $g=2$ with the characteristic splitting into six lines. Additional lines result from semi-forbidden transitions that have a lower intensity. A more extensive description of Mn^{2+} EPR of proteins has been published previously.[20] The EPR spectrum of Mn^{2+} bound aldolase is dominated by the characteristic six line pattern around $g=2$, with a hyperfine coupling constant of circa 95 Gauss. This hyperfine coupling constant is consistent with an octahedral Mn^{2+} complex with mixed oxygen ligands.[26] Association of potentially bidentate binding aldehyde acceptors (glycolaldehyde, methylglyoxal) did not significantly alter the EPR spectrum of the holoenzyme (Figure S33), while the donor substrates pyruvate and hydroxypyruvate considerably changed the EPR signal (Figure 4, top). The ketoacid functional group is therefore required for coordination and activation of the donor substrate. Pyruvate dramatically altered the spectrum, as the higher order spin transitions with $\Delta m_s=1$ became dominant. The EPR spectrum of pyruvate bound Mn-*Sw*HKA exhibits features at $g=1.13$, 1.44 2.16, 2.81 and 4.3 that represent higher order spin transitions. The feature around $g=4.3$ exhibits the characteristic 6-line pattern with a hyperfine coupling constant of circa 95 Gauss. This is indicative of a large change in the electronic structure of the Mn^{2+} ion, which would result from a change in the coordination number and geometry. The change after addition of hydroxypyruvate is subtler, but significant and in agreement with the bidentate coordination of hydroxypyruvate in the crystal structure of Mg^{2+}-*Sw*HKA. Most importantly, addition of phosphate to the holoenzyme both in the presence and absence of substrate did not alter the EPR spectra (Figure 4, bottom), which confirmed our previous notion that there is no direct interaction between the metal and phosphate in the active site. A similar change in the zero-field splitting has previously been reported for the Mn(II) bound extradiol cleaving catechol dioxygenase upon the addition of the substrate 3,4-dihydroxyphenylacetate and for Mn(II) bound pyruvate kinase upon the addition of pyruvate or phosphoenolpyruvate.[27] Spectra similar to the pyruvate bound Mn-*Sw*HKA have also been reported for

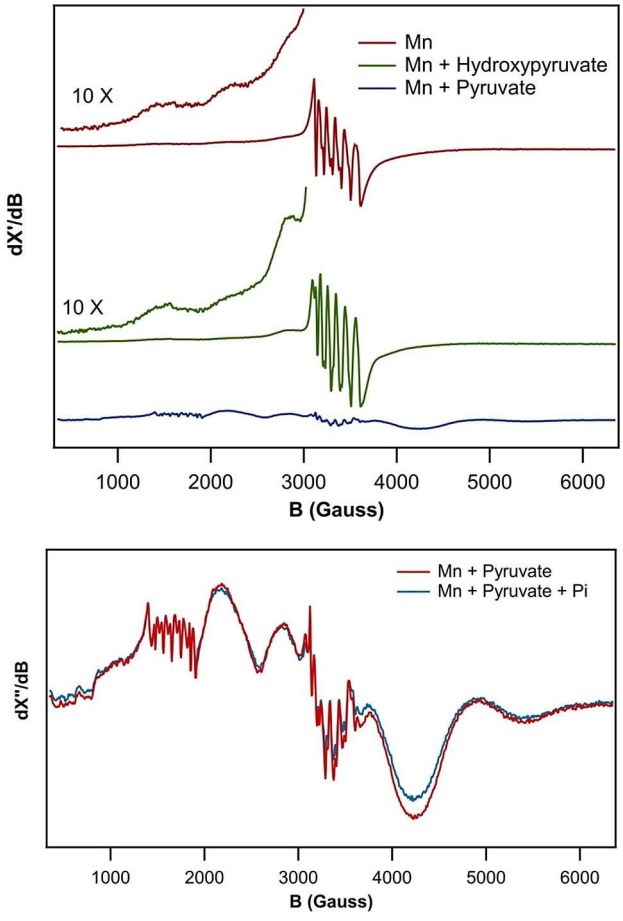

Figure 4. EPR spectroscopy of Mn(II) bound aldolase, showing the effect of donor substrates on the spectrum of Mn^{2+}-*Sw*HKA (top) and no effect by the addition of KPi (bottom). EPR conditions: microwave frequency, 9.402 GHz; microwave power, 0.2 mW; modulation frequency, 100 kHz; modulation amplitude, 10 Gauss; temperature,

oxalate decarboxylase, oxalate oxidase, hydroxynitrile lyase *Gt*HNL and phosphoglucosemutase.[20,28]

Kinetic Analysis of Phosphate Activation

On a mechanistic level, the aldol reaction between (hydroxy-)pyruvate and an aldehyde acceptor is fully reversible *via* the same reaction pathway and comprises of three distinct reaction steps, starting from the bound substrate (Michaelis complex, Scheme 2). These

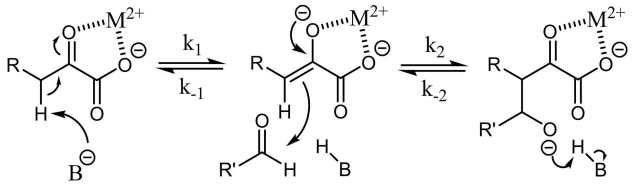

Scheme 2. Discrete reaction steps during the aldol reaction of (hydroxy-) pyruvate and an acceptor aldehyde. The corresponding thermodynamic equilibria can also be described by the associated rate constants in the forward and reverse direction.

steps are characterised by their corresponding rate constants (k_1–k_3 and k_{-1}–k_{-3}). The reaction is initialised by deprotonation at C3 in the donor substrate (k_1) to afford an enolate intermediate. Nucleophilic attack on the aldehyde then creates a new C–C bond (k_2) and final protonation of the alkoxide closes the catalytic cycle (k_3, for simplicity not shown).

In deuterated buffers, the enzyme catalyses the H–D exchange in the donor substrate in the absence of aldehydes (Scheme 3), which allows to specifically study the impact of phosphate on the kinetic rate constants of (de-)protonation (k_1 and k_{-1}).

The aldolase catalysed decarboxylation of oxaloacetate then represents an extended model system, which also takes the C–C bond forming/breaking step (k_2 and k_{-2}) into account (Scheme 4). In this case,

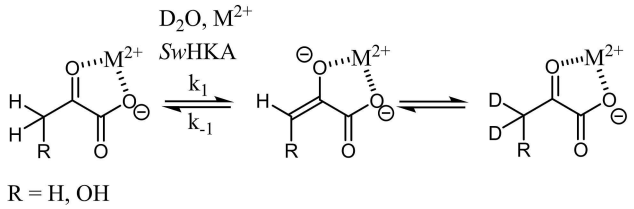

Scheme 3. *Sw*HKA catalysed H–D exchange in (hydroxy-) pyruvate in deuterated buffers using the non-paramagnetic Mg^{2+} as metal cofactor. This allows to specifically study enolisation as the first step in the aldol reaction. Complete exchange was observed for all enzyme variants, indicating no strict preference for the enantiotopic hydrogens when R=OH.

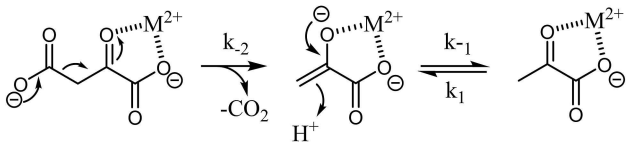

Scheme 4. *Sw*HKA catalysed retro-aldol type decarboxylation of oxaloacetate. C–C bond breaking (k_{-2}) directly affords the enol intermediate and the subsequent protonation step corresponds to rate constant k_{-1}.

irreversible C–C bond breaking (decarboxylation, $K_{eq} = 1.36 \times 10^6$ at pH 7.5, Table S2) effects the direct formation of the active enolate species. Subsequent protonation of the enolate intermediate (k_{-1}) then affords the final product pyruvate.

Remarkably, the presence of phosphate increases the initial rate of H–D exchange in pyruvate by 120-fold (Figure S31). In contrast, the K_M for oxaloacetate was unaffected by the presence of phosphate, while the catalytic rate constant k_{cat} only increased 10-fold. Phosphate therefore does not improve the binding of the substrate, but exclusively increases its rate of decarboxylation. In summary, these findings indicate that when oxaloacetate is used as substrate, (de-) protonation is rate-limiting in the absence of phosphate, while C–C bond formation/breaking becomes rate limiting in its presence. For acceptor substrates, where electronic effects or steric constraints do not already render C–C bond formation rate limiting to begin with, a theoretical rate enhancement of up to 120-fold could be achieved by increasing the rate of enolisation when phosphate saturated conditions are used.

CH-π Interactions

Since *Sw*HKA was previously shown to be particularly good at utilising HPA in aldol reactions, its active site geometry was compared to a previously published model of active site conservation among the 19 class II pyruvate aldolases that were found to be active towards HPA.[10] While highly similar, residue F210 in *Sw*HKA occupies the position of a generally conserved leucine residue as the sole apparent deviation from the model. A similarly positioned phenylalanine residue was previously reported for the class I KDPG aldolase, where the authors described its function to cap the pyruvate methyl group.[29] In carbohydrate utilising enzymes, CH-π interactions between aromatic residues and electropositive saccharide C–H bonds have been extensively investigated and are considered one of the key determinants for carbohydrate recognition in proteins.[17,30] Briefly, electron rich aromatic systems donate electron density into electropositive C–H bonds, thereby establishing binding interactions that compensate for the mismatch in polarity. In analogy to

carbohydrate utilising enzymes, we therefore hypothesised that CH-π interactions between F210 and the C–H bonds at C3 in HPA are responsible for its efficient conversion by *Sw*HKA. To provide evidence for our hypothesis, we created the variant F210L as a representative of the conserved active site geometry of pyruvate aldolases[10] and two variants F210Y and F210W which possess higher electron densities in their aromatic system than phenylalanine.[17] To our surprise, all variants were comparably able to catalyse the formation of the enol intermediate from hydroxypyruvate during H–D exchange experiments (Figure 5), where variant

F210L showed 50% and F210Y 175% relative activity with respect to the WT. The F210W mutant was only slightly better than F210L and showed 60% relative activity, which could either be due to its steric constraints, or binding interactions which are too strong for efficient turnover. Nevertheless, substantial differences were observed when the previously reported conversion of hydroxypyruvate with DL-glyceraldehyde[10] was followed over time. Equilibrium conditions were reached within 30 minutes and 1.5 hours for the F210Y mutant and the WT respectively, whereas the F210L mutant took 72 hours (Figure S37). To rule out any possible effects from the acceptor substrate, the conversion of DL-glyceraldehyde with pyruvate was followed under identical conditions. In this case, no apparent difference was observed between F210L and the WT, demonstrating that the observed effect indeed originated from the different donor substrates (Figure S36–S39). Soaking of Mg^{2+}-*Sw*HKA crystals with hydroxypyruvate showed that both C–H bonds at C3 indeed are oriented towards the aromatic system of F210 for CH-π interactions and revealed a hydrogen bond between the substrate's hydroxyl group and the backbone carbonyl of I167 (Figure 1). In this configuration, the hydroxyl group is oriented towards the inside of the active site, preventing it from blocking the narrow substrate channel.

Upon deprotonation, the enol intermediate then adopts a planar configuration and docking studies suggest a newly formed hydrogen bond between the hydroxyl group and R69, alongside CH-π interactions of the olefinic hydrogen with F210 (Figure 6). This geometry allows for the acceptor substrate to freely converge towards the nucleophile and facilitates C–C bond formation. In the F210Y mutant, the phenolic hydroxyl group is too far away for direct interactions with the substrate and the observed increase in H–D exchange rate must therefore originate from enhanced CH-π interactions. Based on the configuration of L216 in the DDG aldolase (1dxf.pdb, rmsd = 1.61 Å), the F210L mutation was modelled *in silico* as the corresponding rotamer. The model revealed steric clashes between the isobutyl side chain and the hydroxyl group, which would prevent both hydroxypyruvate and the enol intermediate from adopting similar configurations (Figure S42). While the F210L mutant can catalyse the first step in the aldol reaction, it subsequently seems to trap the enol intermediate in a disfavoured configuration that hinders C–C bond formation.

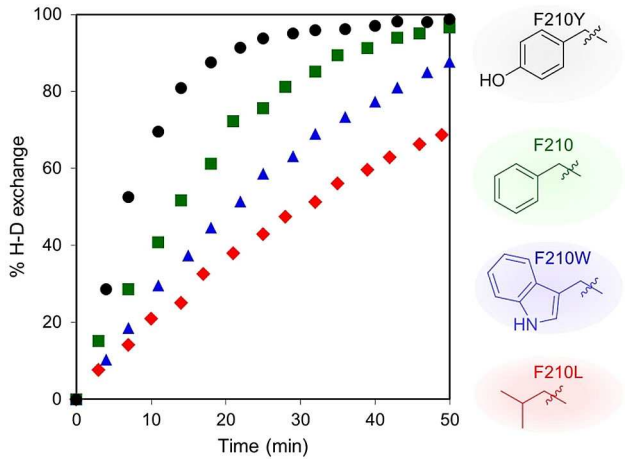

Figure 5. Enzyme catalysed H–D exchange in hydroxypyruvate by *Sw*HKA F210X mutants in deuterated buffer (5 mM KPi, pD = 7.4). Control experiments in the absence of enzyme showed < 1% background exchange over the investigated time frame.

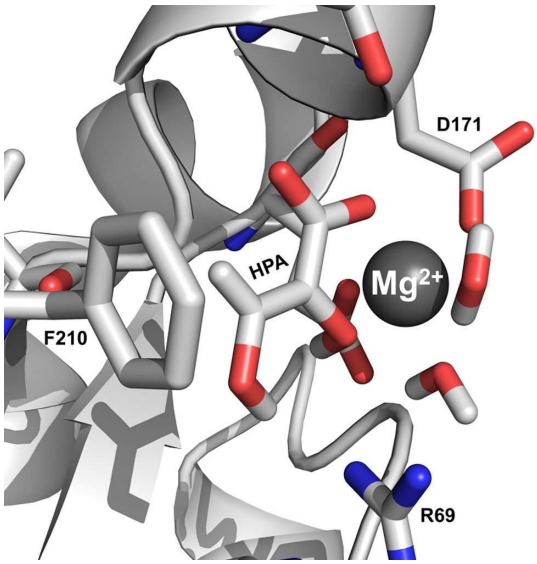

Figure 6. Docking of the planar enol intermediate from HPA into the active site of Mg^{2+}-*Sw*HKA (6r62.pdb) with YASARA. CH-π interactions are established between F210 and the olefinic C–H bond at C3 in HPA and the hydroxyl group forms a H-bond to R69. For simplicity, the second monomer has been omitted. Figures were created with PyMOL.[16]

Conclusion

In summary, this characterization of the *Sw*HKA aldolase A5VH82 has yielded new insights into the enzyme's kinetic properties and the mode of phosphate binding and activation. Due to the lack of proximal amino acid residues, a structural molecule of water was previously identified to be responsible for deprotonation of the substrate. However, this water molecule is only insufficiently activated by the adjacent residues and renders deprotonation of the donor substrate rate limiting. Alternatively, this enzyme can bind inorganic phosphate *via* H44 with high affinity, which replaces water as the catalytic base and results in a rate enhancement of up to 120-fold. Since C–C bond formation becomes rate limiting under phosphate saturated conditions, the overall obtained rate enhancement then depends on the kinetic properties of the acceptor substrate. Our results highlight a common pitfall that is responsible for the previous misconception of the effect of phosphate in class II pyruvate aldolases: excessive phosphate concentrations negatively affect the reaction rate by removing the metal cofactor. We demonstrated that phosphate activation is not a unique property of the αββα sandwich fold, but also is functionally conserved within the same order of magnitude in the distinct $(\alpha/\beta)_8$ barrel fold of the *Sw*HKA aldolase. Future research into class II pyruvate aldolases should therefore take the possibility of phosphate activation into account. While the conserved variant F210L efficiently catalyses the first step of the aldol reaction to generate the enol intermediate from HPA, its configuration hinders subsequent C–C bond formation. So far, CH-π interactions have mainly been investigated for carbohydrate active enzymes. Our findings now illustrate their importance for another enzyme class, where they allow for the conversion of a non-natural substrate. By further increasing the electron density of the aromatic system in the F210Y mutant, we obtained a variant of 2-fold improved activity. CH-π interactions should therefore also be included in rational enzyme design strategies when electropositive C–H bonds are involved.

Experimental Section

Detailed protocols for the enzyme expression, purification and the corresponding gene sequences are provided next to additional graphs in the electronic supporting information.

Chemicals were generally bought in the highest purity commercially available and were used without further purification, unless stated otherwise.

General Oxaloacetate Decarboxylase Activity Assay

*Sw*HKA aldolase was incubated with NADH (0.5 mM), M^{2+} (1 mM), L-Lactic dehydrogenase type II (LDH, from rabbit muscle, 10 U/mL, as ammonium sulphate suspension, Sigma Aldrich) in triethanolamine buffer (TEOA, 5 mM, pH = 7.5) and the reaction was initiated by the addition of oxaloacetate (0.5 mM) to give a final volume of 1 mL. The change in absorbance was followed at 340 nm in PMMA cuvettes (800 rpm, 25 °C) in triplicate, using a Cary 60 UV-Vis spectrometer (Agilent Technologies) equipped with a TC 1 stirring unit (Quantum Northwest). Curve fitting was performed with IGOR, assuming Michaelis-Menten type kinetics.

Measurement of Inorganic Phosphate

Ammonium molybdate (1.5 g, 12% w/v) was dissolved in 6 M sulfuric acid (125 mL). The assay solution was freshly prepared from sodium ascorbate (0.2 g in 10 mL H_2O), sodium dodecylsulfate (1.25 mL, 10% in H_2O) and ammonium molybdate solution (1.25 mL). 400 µL sample were mixed with 600 µL assay solution, incubated for 10 minutes at room temperature and the absorbance was measured at 750 nm.

EPR

EPR measurements were carried out using a Bruker EMXplus 9.5 spectrometer and the following conditions: 9.402 GHz microwave frequency, 0.2 mW microwave power, 100 kHz modulation frequency, 10 Gauss modulation amplitude at a temperature of 37 K. The microwave power was optimized by recording a 2D powerplot from 0 to 40 dB using the Xenon software (Bruker), which was analysed using a labview EPR analysis program written by W.R. Hagen (to be published elsewhere). The low temperature was maintained by boiling liquid helium and the cold helium vapour was passed through a double wall quartz glass tube which was mounted and fitted in the rectangular cavity.[31] Samples were prepared in TEOA buffer (5 mM, pH = 7.5) to contain 1.2 mM of purified apoenzyme (calculated for the molecular weight of the monomer of 27.4 kDa), Mn^{2+} (1 mM, 0.85 eq.), KPi (2 mM, 1.7 eq.) ketoacids/aldehyde substrate (10 mM, 8.3 eq.) to afford a final volume of 200 µL.

H-D Exchange

NMR spectra were recorded using an Agilent 400 MHz (^{1}H, 9.4 Tesla) spectrometer operating at 399.67 MHz for ^{1}H at 298 K and were subsequently interpreted using MestReNova. A benzene-D_6 capillary (Sigma-Aldrich) was used for external locking and quantitation during water suppression experiments with the PRESAT-PURGE pulse sequence. Spectra were recorded using a recycle delay of 2 seconds and 32 repetitions. *Sw*HKA (1.25 mg/mL) was incubated with Mg^{2+} (2 mM) in potassium phosphate buffer (5 mM, pD = 7.4, prepared in D_2O, lyophilised and re-dissolved in D_2O). The reaction was initialised by the addition of ketoacid substrate (50 mM). Controls in the absence of enzyme under identical conditions showed < 1% chemical background activity over the investigated time frame.

Aldol Reactions of (Hydroxy-) Pyruvate with DL-Glyceraldehyde

*Sw*HKA (0.5 mg/mL) was incubated with Mg^{2+} (2 mM), DL-glyceraldehyde (50 mM) and the reaction was initialised by the addition of ketoacid substrate (50 mM) in potassium phosphate buffer (5 mM, pH 7.0, 1.5 mL, 25 °C, 500 rpm). Samples were quenched by 1:1 dilution with trifluoroacetic acid (TFA, 0.2% v/v in H_2O) and the enzyme was precipitated by centrifugation. Concentrations were determined by RP-HPLC (ICSep ICE Coregel-87H3 column, 0.4 × 25 cm, Transgenomic, 0.1% v/v TFA, 0.8 mL/min, 60 °C, 210 nm) on a Shimadzu LC-20AD system using external standards.

Crystallisation and Data Collection

Well diffracting crystals of apo-*Sw*HKA protein were obtained at 277 K using the vapour diffusion method, from drops resulting from mixing equal volumes of a protein sample at 9.2 mg/ml with a crystallization solution consisting of 0.44 M to 0.65 M of sodium citrate and 0.1 M HEPES (4-(2-hydroxyethyl)-1-piperazineethanesulfonic acid) at pH 7.05. Crystals took 7 days to appear and grew to their final size within a few days. Crystals of the holo-*Sw*HKA in complex with hydroxypyruvate were obtained by transferring crystals of apo-*Sw*HKA into a new drop containing 0.7 M of potassium bromide (KBr), 0.1 M HEPES pH 7.05, 20 mM of magnesium chloride ($MgCl_2$) and 150 mM of hydroxypyruvate. The crystals were left in this new condition for a few hours and then were cryo-cooled using as cryoprotectant 20% of glycerol. X-ray diffraction data was collected at beamline P13 operated by EMBL Hamburg at the PETRA III storage ring (DESY, Hamburg, Germany).[32] The protein crystallized in the cubic space group P 42 3 2, with unit-cell parameters of approx. a = 116.6 Å, with one molecule in the asymmetric unit and a solvent content of 47.5%.

Structure Solution and Refinement

Data were indexed and integrated with XDS,[33] scaled with AIMLESS,[34] and the space group was determined with POINTLESS[35] from CCP4 programs suite.[36] Data-collection statistics are given in Table S1. The structure was solved by the molecular-replacement method with the program MOLREP[37] using the crystal structure of apo-*Sw*HKA as a search model (unpublished data). Model building and refinement of ligand bound holo-*Sw*HKA was performed with COOT[38] and PHENIX,[39] respectively. The program PHENIX was used to refine atomic coordinates together with individual isotropic atomic displacement parameters. TLS thermal anisotropic parameterization was also included in the final stages of refinement, with each monomeric subunit divided into three TLS groups, as suggested by TLS Motion Determination.[38,40] A randomly selected 5% of observed reflections were kept aside during refinement for cross-validation. The positions of the magnesium ion and of the hydroxypyruvate became evident after the first cycles of refinement, based on electron density difference maps, and both entities were modelled and refined with full occupancy. Solvent molecules were included in the model after a few rounds of refinement as well as bromide and potassium ions that were located at the surface of the protein. Structure refinement statistics are listed in Table S1.

Substrate Docking

A simulation cell of 9 Å was defined around R69 in the crystal structure of Mg^{2+}-*Sw*HKA (6r62.pdb). The enol intermediate (2,3-dihydroxy acrylic acid) was energy minimised (MM2 calculation, Chem3D 15.1) and subsequently docked into the active site using YASARA (dock_run.mcr, version 16.12.29). A structural model for variant F210L was created *in silico* based on the rotamer orientation of L216 in the DDG pyruvate aldolase (1dxf.pdb) and the enol intermediate was docked into the model following the same approach.

Acknowledgements

We would like to thank Stephen J. Eustace, Lloyd Mallée, Marc Strampraad, Laura van der Weel and Remco van Oosten for their technical support.

References

[1] a) K. Hernández, J. Joglar, J. Bujons, T. Parella, P. Clapés, *Angew. Chem. Int. Ed.* **2018**, *57*, 3583–3587; b) K. Hernandez, J. Bujons, J. Joglar, S. J. Charnock, P. Dominguez de Maria, W. D. Fessner, P. Clapés, *ACS Catal.* **2017**, *7*, 1707–1711.

[2] V. Laurent, E. Darii, A. Aujon, M. Debacker, J.-L. Petit, V. Hélaine, T. Liptaj, M. Breza, A. Mariage, L. Nauton, M. Traïkia, M. Salanoubat, M. Lemaire, C. Guérard-Hélaine, V. de Berardinis, *Angew. Chem.* **2018**, *130*, 5565–5569.

[3] a) W. A. Greenberg, A. Varvak, S. R. Hanson, K. Wong, H. Huang, P. Chen, M. J. Burk, *Proc. Natl. Acad. Sci. USA* **2004**, *101*, 5788–5793; b) J. Wagner, R. A. Lerner, C. F. Barbas, *Science* **1995**, *270*, 1797–1800; c) C. F. Barbas, A. Heine, G. Zhong, T. Hoffmann, S. Gramatikova, R. Björnestedt, B. List, J. Anderson, E. A. Stura, I. A. Wilson, *Science* **1997**, *278*, 2085–2092; d) R. N. Patel, in *Organic Synthesis Using Biocatalysis*, Elsevier, **2015**, pp. 339–411.

[4] A. Liese, K. Seelbach, A. Buchholz, J. Haberland, in *Industrial Biotransformations*, second ed. (Eds.: A. Liese, K. Seelbach, C. Wandrey), Wiley-VCH, **2006**, p. 459.

[5] a) C.-H. Wong, G. M. Whitesides, *Enzymes in synthetic organic chemistry, Vol. 12*, Academic Press, **1994**; b) A. Bolt, A. Berry, A. Nelson, *Arch. Biochem. Biophys.* **2008**, *474*, 318–330; c) P. Clapés, in *Science of Synthesis Biocatalysis in Organic Synthesis 2* (Ed.: W.-D. F. K. Faber, N. J. Turner), Georg Thieme Verlag, Stuttgart, **2015**, pp. 31–93; d) J. Sukumaran, U. Hanefeld, *Chem. Soc. Rev.* **2005**, *34*, 530–542; e) A. Ranoux, U. Hanefeld, in *Stereoselective Synthesis of Drugs and Natural Products*, First ed. (Ed.: V. Andrushko, N. Andrushko), John Wiley & Sons, **2013**, pp. 831–857.

[6] B. Horecker, O. Tsolas, C. Lai, in *The enzymes, Vol. 7*, Elsevier, **1972**, pp. 213–258.

[7] a) D. E. Morse, B. Horecker, *Advances in Enzymology and Related Areas of Molecular Biology, Volume 31*

1968, 125–181; b) W. Rutter, in *Fed. Proc., Vol. 23*, **1964**, pp. 1248–1257.
[8] a) K. Furukawa, J. Hirose, A. Suyama, T. Zaiki, S. Hayashida, *J. Bacteriol.* **1993**, *175*, 5224–5232; b) K. Furukawa, N. Kimura, *Environ. Health Perspect.* **1995**, *103*, 21–23; c) J.-S. Seo, Y.-S. Keum, Y. Hu, S.-E. Lee, Q. X. Li, *Biodegradation* **2007**, *18*, 123–131; d) E. Masai, Y. Katayama, M. Fukuda, *Biosci. Biotechnol. Biochem.* **2007**, *71*, 1–15.
[9] a) P. Baker, S. Y. K. Seah, *J. Am. Chem. Soc.* **2011**, *134*, 507–513; b) M. Cheriyan, M. J. Walters, B. D. Kang, L. L. Anzaldi, E. J. Toone, C. A. Fierke, *Bioorg. Med. Chem.* **2011**, *19*, 6447–6453; c) M. J. Walters, E. J. Toone, *Nat. Protoc.* **2007**, *2*, 1825–1830.
[10] V. de Berardinis, C. Guérard-Hélaine, E. Darii, K. Bastard, V. Hélaine, A. Mariage, J.-L. Petit, N. Poupard, I. Sánchez-Moreno, M. Stam, T. Gefflaut, M. Salanoubat, M. Lemaire, *Green Chem.* **2017**, *19*, 519–526.
[11] T. Izard, N. C. Blackwell, *EMBO J.* **2000**, *19*, 3849–3856.
[12] W. Wang, S. Y. K. Seah, *Biochemistry* **2005**, *44*, 9447–9455.
[13] W. Wang, S. Mazurkewich, M. S. Kimber, S. Y. K. Seah, *J. Biol. Chem.* **2010**, *285*, 36608–36615.
[14] S. Mazurkewich, S. Y. K. Seah, *PLoS One* **2016**, *11*, e0164556.
[15] M. Coincon, W. Wang, J. Sygusch, S. Y. K. Seah, *J. Biol. Chem.* **2012**, *287*, 36208–36221.
[16] W. L. DeLano, *http://www.pymol.org*, **2002**.
[17] K. L. Hudson, G. J. Bartlett, R. C. Diehl, J. Agirre, T. Gallagher, L. L. Kiessling, D. N. Woolfson, *J. Am. Chem. Soc.* **2015**, *137*, 15152–15160.
[18] a) A. C. Joerger, C. Gosse, W.-D. Fessner, G. E. Schulz, *Biochemistry* **2000**, *39*, 6033–6041; b) S. J. Cooper, G. A. Leonard, S. M. McSweeney, A. W. Thompson, J. H. Naismith, S. Qamar, A. Plater, A. Berry, W. N. Hunter, *Structure* **1996**, *4*, 1303–1315; c) M. Kroemer, I. Merkel, G. E. Schulz, *Biochemistry* **2003**, *42*, 10560–10568.
[19] a) S. Kobayashi, S. Nagayama, T. Busujima, *J. Am. Chem. Soc.* **1998**, *120*, 8287–8288; b) S. Kobayashi, K. Manabe, *Acc. Chem. Res.* **2002**, *35*, 209–217.
[20] F. Vertregt, G. Torrelo, S. Trunk, H. Wiltsche, W. R. Hagen, U. Hanefeld, K. Steiner, *ACS Catal.* **2016**, *6*, 5081–5085.
[21] O. C. Richards, W. J. Rutter, *J. Biol. Chem.* **1961**, *236*, 3177–3184.
[22] a) W. Wang, S. Y. K. Seah, *FEBS Lett.* **2008**, *582*, 3385–3388; b) P. Baker, J. Carere, S. Y. K. Seah, *Biochemistry* **2011**, *50*, 3559–3569; c) D. Rea, R. Hovington, J. F. Rakus, J. A. Gerlt, V. Fülöp, T. D. H. Bugg, D. I. Roper, *Biochemistry* **2008**, *47*, 9955–9965; d) D. Rea, V. Fülöp, T. D. H. Bugg, D. I. Roper, *J. Mol. Biol.* **2007**, *373*, 866–876; e) G.-T. Huang, J.-S. K. Yu, *ACS Catal.* **2017**, *7*, 8130–8133.
[23] a) N. S. Chickerur, G. H. Nayak, R. C. Lenka, P. P. Mahapatra, *Thermochim. Acta* **1982**, *58*, 111–115; b) N. E. Good, G. D. Winget, W. Winter, T. N. Connolly, S. Izawa, R. M. M. Singh, *Biochemistry* **1966**, *5*, 467–477.
[24] M. E. B. Smith, K. Smithies, T. Senussi, P. A. Dalby, H. C. Hailes, *Eur. J. Org. Chem.* **2006**, *2006*, 1121–1123.
[25] S. R. Marsden, L. Gjonaj, S. J. Eustace, U. Hanefeld, *ChemCatChem* **2017**, *9*, 1808–1814.
[26] A. K. Whiting, Y. R. Boldt, M. P. Hendrich, L. P. Wackett, L. Que, *Biochemistry* **1996**, *35*, 160–170.
[27] a) A. K. Whiting, Y. R. Boldt, M. P. Hendrich, L. P. Wackett, L. Que, *Biochemistry* **1996**, *35*, 160–170; b) G. H. Reed, S. D. Morgan, *Biochemistry* **1974**, *13*, 3537–3541.
[28] P. Campomanes, W. F. Kellett, L. M. Easthon, A. Ozarowski, K. N. Allen, A. Angerhofer, U. Rothlisberger, N. G. J. Richards, *J. Am. Chem. Soc.* **2014**, *136*, 2313–2323.
[29] S. W. B. Fullerton, J. S. Griffiths, A. B. Merkel, M. Cheriyan, N. J. Wymer, M. J. Hutchins, C. A. Fierke, E. J. Toone, J. H. Naismith, *Bioorg. Med. Chem.* **2006**, *14*, 3002–3010.
[30] a) W. Chen, S. Enck, J. L. Price, D. L. Powers, E. T. Powers, C.-H. Wong, H. J. Dyson, J. W. Kelly, *J. Am. Chem. Soc.* **2013**, *135*, 9877–9884; b) M. d. C. Fernández-Alonso, F. J. Cañada, J. Jiménez-Barbero, G. Cuevas, *J. Am. Chem. Soc.* **2005**, *127*, 7379–7386; c) J. L. Asensio, A. Ardá, F. J. Cañada, J. Jiménez-Barbero, *Acc. Chem. Res.* **2013**, *46*, 946–954; d) M. I. Chávez, C. Andreu, P. Vidal, N. Aboitiz, F. Freire, P. Groves, J. L. Asensio, G. Asensio, M. Muraki, F. J. Cañada, J. Jiménez-Barbero, *Chem. Eur. J.* **2005**, *11*, 7060–7074.
[31] a) I. Salmeen, G. Palmer, *J. Chem. Phys.* **1968**, *48*, 2049–2052; b) A. Lundin, R. Aasa, *J. Magn. Reson.* **1972**, *8*, 70–73.
[32] M. Cianci, G. Bourenkov, G. Pompidor, I. Karpics, J. Kallio, I. Bento, M. Roessle, F. Cipriani, S. Fiedler, T. R. Schneider, *J. Synchrotron Radiat.* **2017**, *24*, 323–332.
[33] W. Kabsch, *Acta Crystallogr. Sect. D* **2010**, *66*, 125–132.
[34] P. R. Evans, *Acta Crystallogr. Sect. D* **2011**, *67*, 282–292.
[35] P. R. Evans, G. N. Murshudov, *Acta Crystallogr. Sect. D* **2013**, *69*, 1204–1214.
[36] Collaborative Computational Project, Number 4, *Acta Crystallogr. Sect. D Biol. Crystallogr.* **1994**, *50*, 760–763.
[37] A. Vagin, A. Teplyakov, *J. Appl. Crystallogr.* **1997**, *30*, 1022–1025.
[38] J. Painter, E. A. Merritt, *Acta Crystallogr. Sect. D* **2005**, *61*, 465–471.
[39] P. D. Adams, P. V. Afonine, G. Bunkóczi, V. B. Chen, I. W. Davis, N. Echols, J. J. Headd, L.-W. Hung, G. J. Kapral, R. W. Grosse-Kunstleve, A. J. McCoy, N. W. Moriarty, R. Oeffner, R. J. Read, D. C. Richardson, J. S. Richardson, T. C. Terwilliger, P. H. Zwart, *Acta Crystallogr. Sect. D* **2010**, *66*, 213–221.
[40] M. D. Winn, M. N. Isupov, G. N. Murshudov, *Acta Crystallogr. Sect. D* **2001**, *57*, 122–133.

